

Amphiphilic Polypyridyl Ruthenium Complexes with Substituted 2,2'-Dipyridylamine Ligands for Nanocrystalline Dye-Sensitized Solar Cells

Peng Wang, Robin Humphry-Baker, Jacques E. Moser, Shaik M. Zakeeruddin,* and Michael Grätzel*

Laboratory for Photonics & Interfaces, Swiss Federal Institute of Technology, CH-1015 Lausanne, Switzerland

Received January 22, 2004. Revised Manuscript Received May 10, 2004

Two heteroleptic polypyridyl ruthenium complexes $[\text{Ru}(\text{dcbpy})(\text{L})(\text{NCS})_2]$, where dcbpy is 4,4'-dicarboxylic acid-2,2'-bipyridine and L is *N,N*-di(2-pyridyl)-dodecylamine or *N,N*-di(2-pyridyl)-tetradecylamine] have been synthesized and characterized by elemental analysis, voltammetry, ^1H NMR, UV-vis, ATR-FTIR, and resonance Raman spectroscopies. Resonance Raman studies have revealed that the lowest unoccupied molecular orbital (LUMO) of the two sensitizers is localized on the dcbpy-ligand-bearing anchoring group. Nanosecond laser transient measurements have shown that dye regeneration by iodide in the electrolyte can efficiently compete with the recombination reaction of injected electrons trapped in the nanocrystalline TiO_2 film with dye molecules in the oxidized state. Furthermore, these amphiphilic ruthenium complexes were successfully used as sensitizers for nanocrystalline dye-sensitized solar cells with efficiencies of 8.2% at the 100 mW cm^{-2} irradiance of air mass 1.5 solar light and $\geq 8.7\%$ at lower light intensities.

Introduction

Nanocrystalline dye-sensitized solar cells (DSCs) are attracting considerable interest due to their high efficiency and potential application as cost-effective alternatives to present p-n junction photovoltaic devices.¹ One of the major strategies to achieve total power conversion efficiency over 10% is the development of new sensitizers to harvest a larger portion of the solar spectrum.² Some polypyridyl ruthenium(II) complexes have been used as efficient sensitizers because they have an intense metal-to-ligand charge transfer (MLCT) transition in the visible region to absorb the solar radiation. These MLCT transitions are from the metal t_{2g} orbital to the π^* orbital of the ligand. Another advantage of using ruthenium sensitizers is their relative stability in the oxidized and reduced forms and the ease of tuning their spectral, photophysical, and electrochemical properties by introducing an appropriate ligand in a controlled manner. Two strategies have been successfully applied in designing ruthenium complexes to absorb the whole visible spectrum, including lifting the HOMO (highest occupied molecular orbital) level by incorporating strong σ -donor ligands or lowering the LUMO (lowest unoccupied molecular orbital) level of the anchoring ligands.³

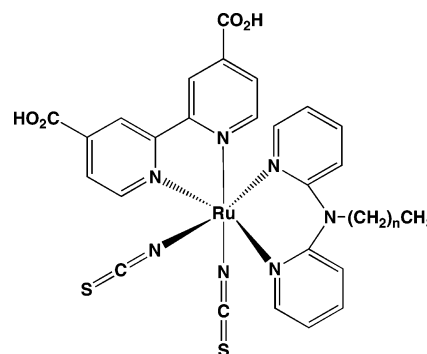


Figure 1. Molecular structures of complex **I** ($n = 13$) and complex **II** ($n = 11$).

Dipyridylamine (DPA-H), or its alkyl-substituted derivatives (DPA-R), is an aromatic amine in some ways similar to 2,2'-bipyridine (bpy). Their difference lies in that the former forms a 6-member ring with less π -acceptor character on chelation rather than a 5-member ring for bpy (see Figure 1). Also, due to the lone-pair electrons of the amine it is more σ -electron donating than the bpy ligand. The *N*-deprotonated form of DPA has been widely used as a building block for the synthesis of metal-metal bonded binuclear and linear trinuclear complexes.⁴ Their ruthenium complexes have also been reported.⁵

* To whom correspondence should be addressed. E-mail: shaik.zakeer@epfl.ch and michael.graetzel@epfl.ch.

(1) (a) O'Regan, B.; Grätzel, M. *Nature* **1991**, *353*, 737. (b) Hagfeldt, A.; Grätzel, M. *Chem. Rev.* **1995**, *95*, 49. (c) Hagfeldt, A.; Grätzel, M. *Acc. Chem. Res.* **2000**, *33*, 269. (d) Grätzel, M. *Nature* **2001**, *414*, 338.

(2) (a) Nazeeruddin, M. K.; Kay, A.; Rodicio, I.; Humphry-Baker, R.; Müller, E.; Liska, P.; Vlachopoulos, N.; Grätzel, M. *J. Am. Chem. Soc.* **1993**, *115*, 6382. (b) Nazeeruddin, M. K.; Péchy, P.; Renouard, T.; Zakeeruddin, S. M.; Humphry-Baker, R.; Comte, P.; Liska, P.; Cevey, L.; Costa, E.; Shklover, V.; Spiccia, L.; Beacon, G. B.; Bignozzi, C. A.; Grätzel, M. *J. Am. Chem. Soc.* **2001**, *123*, 1613.

(3) Anderson, P. A.; Strouse, G. F.; Treadway, J. A.; Keene, F. R.; Meyer, T. J. *Inorg. Chem.* **1994**, *33*, 3863.

(4) For example: (a) Edema, J. J. H.; Gambarotta, S.; Meetsma, A.; Spek, A. L.; Smeets, W. J. J.; Chiang, M. Y. *J. Chem. Soc., Dalton Trans.* **1993**, 789. (b) Cotton, F. A.; Daniels, L. M.; Murillo, C. A.; Pascual, I. *J. Am. Chem. Soc.* **1997**, *119*, 10223. (c) Suen, M. C.; Wu, Y. Y.; Chen, J. D.; Keng, T. C.; Wang, J. C. *Inorg. Chim. Acta* **1999**, *288*, 82. (d) Cléric, R.; Cotton, F. A.; Jeffrey, P. S.; Murillo, C. A.; Wang, X. *Inorg. Chem.* **2001**, *40*, 1265.

Recently, the significance of using amphiphilic polypyridyl ruthenium sensitizers has been demonstrated to achieve enhanced stability in DSCs at elevated temperatures.⁶ Hence, it is interesting to design new ligands leading to the preparation of new amphiphilic ruthenium sensitizers. The synthesis of *N*-alkyl substituted DPA ligands (DPAR) by substituting the proton of DPAH with an alkyl group (R) is very convenient. Earlier, we synthesized different DPAR ligands with varying aliphatic chain lengths to make osmium complexes and successfully used them as redox mediators in amperometric glucose biosensors.⁷ Here we report the synthesis and characterization of amphiphilic ruthenium(II) complexes containing a DPAR ligand and their photovoltaic performance in DSCs. The molecular structure of the two new complexes [Ru(dcbpy)(L)(NCS)₂], where dcbpy is 4,4'-dicarboxylic acid and L is *N,N*-di-(2-pyridyl)-dodecylamine (DPA-C₁₂) or *N,N*-di-(2-pyridyl)-tetradecylamine (DPA-C₁₄), are shown in Figure 1. The synthetic methodology we used for the synthesis of heteroleptic polypyridyl ruthenium complexes is based on the sequential addition of different polypyridyl ligands to [RuCl₂(p-cymene)]₂.^{6a}

Experimental Section

Reagents. All chemicals and solvents used were of purist quality from Fluka. Guanidinium thiocyanate (GNCS) was obtained from Aldrich. *N*-Methylbenzimidazole (NMBI) was purchased from Aldrich and recrystallized from diethyl ether. 4-Guanidinobutyric acid was converted to its chloride salt (GBAHCl) by treating with hydrochloric acid. The synthesis of DPA-C₁₂ and DPA-C₁₄ were reported in our previous paper.⁷

Synthesis of Complexes I and II. In a typical one-pot synthesis, [RuCl₂(p-cymene)]₂ (0.15 g, 0.25 mmol) was dissolved in DMF (50 mL) and to this solution DPAC₁₄ (0.180 g, 0.50 mmol) was added. The reaction mixture was heated to 60 °C under nitrogen for 4 h with constant stirring. To this reaction flask H₂dcbpy (0.12 g, 0.50 mmol) was added and refluxed for a further 4 h. Finally, an excess of NH₄NCS (13 mmol) was added to the reaction mixture and the reflux continued for another 4 h. The reaction mixture was cooled to room temperature and the solvent was removed by using a rotary-evaporator under vacuum. Water was added to the flask and the insoluble solid was collected on a sintered glass crucible by suction filtration. The solid was washed with water followed by diethyl ether and dried under vacuum. The compound was further purified by loading onto a Sephadex LH-20 column with methanol as eluent. ¹H NMR (δ_H/ppm in CD₃OD): 9.6 (d, 1H), 9.1 (d, 1H), 8.9 (s, 1H), 8.8 (s, 1H), 8.3 (s, 1H), 8.2 (s, 1H), 8.05 (t, 1H), 7.9 (d, 1H), 7.8 (t, 2H), 7.60 (t, 1H), 7.5 (d, 1H), 7.4 (t, 1H), 7.2 (d, 1H), 6.8 (t, 1H), 4.1 (t, 2H), 3.7 (t, 2H), 1.40 (m, 24H), 0.90 (t, 3H). Analytical calculation

for C₃₈H₄₅N₇O₄RuS₂·H₂O: C, 53.90; H, 5.55; N, 11.58%. Found: C, 53.28; H, 5.43; N, 11.62%.

Complex II was synthesized as explained above by using the ligand DPAC₁₂. ¹H NMR (δ_H/ppm in CD₃OD): 9.6 (d, 1H), 9.1 (d, 1H), 8.9 (s, 1H), 8.8 (s, 1H), 8.3 (s, 1H), 8.2 (s, 1H), 8.05 (t, 1H), 7.9 (d, 1H), 7.8 (t, 2H), 7.60 (t, 1H), 7.5 (d, 1H), 7.4 (t, 1H), 7.2 (d, 1H), 6.8 (t, 1H), 4.1 (t, 2H), 3.7 (t, 2H), 1.40 (m, 20H), 0.90 (t, 3H). Analytical calculation for C₃₆H₄₁N₇O₄RuS₂: C, 54.00; H, 5.13; N, 12.25%. Found: C, 53.95; H, 5.17; N, 12.12%.

Spectroscopic Measurements. ATR-FTIR spectra were measured using a FTS 7000 FTIR spectrometer (Digilab, United States). The data reported here were taken with the 'Golden Gate' diamond anvil ATR accessory. Spectra were derived from 64 scans at a resolution of 2 cm⁻¹. The samples were measured under the same mechanical force pushing the samples in contact with the diamond window. No ATR correction has been applied to the data. It also has to be appreciated that this ATR technique probes at most 1 μm of sample depth and that this depends on the sample refractive index, porosity, etc. Some of the spectra show artifacts due to attenuation of light by the diamond window in the 2000 to 2350 cm⁻¹ region. Dye coated films were rinsed in acetonitrile and dried prior to measuring the spectra.

The resonance Raman spectra were obtained using a Coherent INNOVA 200K Kr⁺ laser source and a SPEX 1877 Triplemate with liquid-nitrogen-cooled CCD-1024 detection. Excitation wavelengths were 468.0 and 520.8 nm. All the data reported here were irradiated using a front-face 135° scattering geometry. In this configuration, the laser beam waist at the sample was about 6 μm. The dye samples were measured on TiO₂ anatase films in the dry state and in a sealed DSC cell. Laser-induced sample degradation was minimized by using a low laser power (typically 10 mW) and by spinning the sample in the exciting laser beam. All the data are photometrically corrected using a standard 200 W Halogen lamp. The spectral resolution was typically 2 cm⁻¹. Baseline correction has been applied to the displayed spectra.

UV-vis electronic absorption and fluorescence emission spectra were measured using a Cary 5 spectrophotometer and a Spex Fluorolog 112 spectrofluorimeter, respectively. The emitted light was detected with a Hamamatsu R2658 photomultiplier operated in a single-photon counting mode. The emission spectrum was photometrically corrected with a calibrated 200 W tungsten lamp as reference source.

Electrochemical Measurements. A computer-controlled Autolab P20 electrochemical workstation (Eco Chimie, Netherlands) was used for cyclic and square-wave voltammetric measurements in combination with a conventional three-electrode, one-compartment electrochemical cell. A Pt foil and an Ag/AgCl/KCl_{sat} were used as counter and reference electrodes, respectively. Due to the possible liquid junction potential, the used reference electrode was frequently calibrated by measuring the redox potential of ferrocene. The redox potential values vs calibrated Ag/AgCl/KCl_{sat} were converted to those vs NHE (normal hydrogen electrode). For the electrochemical study of complexes I and II in DMF, a Pt ultramicroelectrode with a radius of 5.0 μm (Bioanalytical Systems, Inc., United States) was used as working electrode. A dye-coated TiO₂ film was used as the working electrode to study the electrochemical behavior of complexes I and II anchored on TiO₂ nanocrystals.

Laser Transient Absorbance Measurements. Dye-coated, 8 μm-thick transparent TiO₂ mesoporous film deposited on flint glass was used for transient absorbance measurements. Nanosecond pulsed laser excitation was applied using a GWU-355 broadband optical parametric oscillator pumped with a Continuum Powerlite 7030 frequency-tripled Q-switched Nd:YAG laser. The oscillator output (30 Hz repetition rate, pulse width at half-height of 5 ns) was tuned at a wavelength of 543 nm and attenuated by filters. To irradiate a large cross-section of the sample, it was kept at a 30° angle to the excitation beam and the beam was expanded by a planoconcave lens. Laser fluence on the sample was kept at a very low level (10 μJ cm⁻² per pulse) to ensure that, on the average, less than one electron is injected per TiO₂ nanopar-

(5) For example: (a) Segers, D. P.; DeArmond, M. K. *J. Phys. Chem.* **1982**, *86*, 3768. (b) Morris, D. E.; Ohsawa, Y.; Segers, D. P.; DeArmond, M. K.; Hanck, K. W. *Inorg. Chem.* **1984**, *23*, 3010. (c) Blakley, R. L.; Myrick, M. L.; DeArmond, M. K. *J. Am. Chem. Soc.* **1986**, *108*, 7843. (d) Anderson, P. A.; Deacon, G. B.; Haarmann, K. H.; Keene, F. R.; Meyer, T. J.; Reitsma, D. A.; Skelton, B. W.; Strouse, G. F.; Thomas, N. C.; Treadway, J. A.; White, A. H. *Inorg. Chem.* **1995**, *34*, 6145. (e) Shepherd, R. E.; Chen, Y.; Kortés, R. A.; Ward, M. S. *Inorg. Chim. Acta* **2000**, *303*, 30. (f) Cabeza, J. A.; del Río, I.; García-Granda, S.; Riera, V.; Suárez, M. *Organometallics* **2002**, *21*, 2540. (g) Chanda, N.; Mobin, S. M.; Puranik, V. G.; Datta, A.; Niemeyer, M.; Lahiri, G. K.; *Inorg. Chem.* **2004**, *43*, 1056.

(6) (a) Wang, P.; Zakeeruddin, S. M.; Moser, J. E.; Nazeeruddin, M. K.; Sekiguchi, T.; Grätzel, M. *Nat. Mater.* **2003**, *2*, 402. (b) Wang, P.; Zakeeruddin, S. M.; Humphry-Baker, R.; Moser, J. E.; Grätzel, M. *Adv. Mater.* **2003**, *15*, 2101.

(7) (a) Saudan, P.; Zakeeruddin, S. M.; Malavallon, M.-A.; Grätzel, M.; Fraser, D. M. *Biotechnol. Bioeng.* **1994**, *44*, 407. (b) Zakeeruddin, S. M.; Grätzel, M.; Fraser, D. M. *Biosens. Bioelectron.* **1996**, *11*, 305.

ticle upon pulsed irradiation. Such conditions are comparable to those prevailing in the functioning of a photovoltaic device. The probe light from a xenon arc lamp was passed first through a monochromator, various optical elements, the sample, and a second monochromator before being detected by a fast photomultiplier tube. Transient absorbance measurements of the dye in the oxidized-state were carried out at a probe wavelength of 650 nm.

Device Fabrication. A screen-printed double layer of TiO₂ particles was used as the photoanode. An 18- μ m thick film of 20-nm sized TiO₂ particles was first printed on the fluorine-doped SnO₂ conducting glass electrode and further coated by a 4- μ m thick second layer of 400-nm diameter, light-scattering anatase particles. The detailed preparation procedures of TiO₂ nanocrystals, pastes for screen-printing, and double-layer nanostructured TiO₂ film have been reported in our previous paper.⁸ A TiO₂ electrode was dye-coated by immersing it in a dye solution containing 300 μ M of complex **I** and 300- μ M GBAHCl in the mixture of acetonitrile and *tert*-butyl alcohol (volume ratio: 1/1) at room temperature for 12 h and then assembled with thermally platinized conducting glass electrodes. The electrodes were separated by a 35- μ m thick Bynel hot-melt gasket (DuPont, United States) and sealed up by heating. The internal space was filled with a liquid electrolyte using a vacuum back filling system. The electrolyte is composed of 0.6 M 1-propyl-3-methylimidazolium, 50 mM I₂, 0.5 M NMBI, and 0.1 M GNCS in the mixed solvent of acetonitrile and valeronitrile (volume ratio: 3/1). The electrolyte-injecting hole made with a sand-blasting drill on the counter electrode glass substrate was sealed with a Bynel sheet and a thin glass cover by heating.

Photoelectrochemical Characterization. A 450 W xenon light source (Oriel, United States) was used to give an irradiance of 100 mW cm⁻² (the equivalent of one sun at air mass (AM) 1.5) at the surface of solar cells. The spectral output of the lamp was matched in the region of 350–750 nm with the aid of a Schott K113 Tempax sunlight filter (Präzisions Glas & Optik GmbH, Germany) so as to reduce the mismatch between the simulated and true solar spectra to less than 2%. Various incident light intensities were regulated with wavelength-neutral wire mesh attenuators. The current–voltage characteristics of the cell under these conditions were obtained by applying external potential bias to the cell and measuring the generated photocurrent with a Keithley model 2400 digital source meter (Keithley, United States). This process was fully automated using Wavemetrics software (<http://www.wavemetrics.com/>). A similar data acquisition system was used to control the incident photon-to-current conversion efficiency (IPCE) measurement. Under full computer control, light from a 300-W xenon lamp (ILC Technology, United States) was focused through a Gemini-180 double monochromator (Jobin Yvon Ltd., United Kingdom) onto the photovoltaic cell under test. The monochromator was incremented through the visible spectrum to generate the IPCE (λ) as defined by $\text{IPCE}(\lambda) = 12400(J_{sc}/\lambda\phi)$, where λ is the wavelength, J_{sc} is short-circuit photocurrent density (mA cm⁻²), and ϕ is the incident radiative flux (mW cm⁻²). Fabricated devices were masked to have an illuminated active area of 0.158 cm² for photoelectrochemical characterization.

Results and Discussion

In the ¹H NMR spectra of heteroleptic polypyridyl ruthenium complexes, the two pyridines in each ligand are necessarily in different magnetic environments. For example, in the ¹H NMR spectrum of complex **I** we see a total of 12 resonance peaks corresponding to aromatic ring protons. Resonance peaks for the aliphatic protons of N-alkyl groups lie in the normal high-field region. Interestingly, the observed two triplets at 3.7 and 4.1

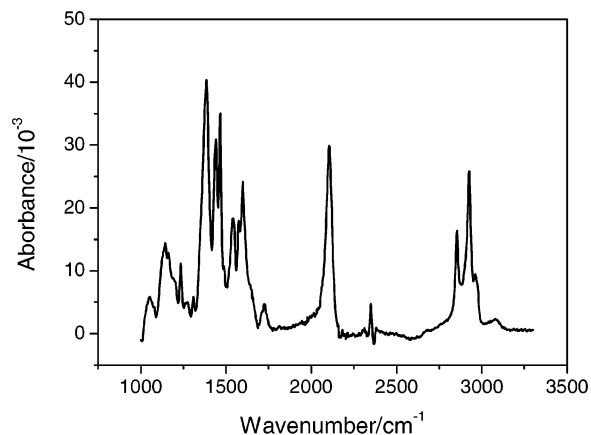


Figure 2. ATR-FTIR spectrum for 6.5- μ m thick mesoporous TiO₂ film coated with complex **I**. A TiO₂ reference film heated to 500 °C has been subtracted for clarity.

ppm corresponding to the N–CH₂ group indicate that it is possible for the lone pair electron of amine to be partly delocalized on aromatic rings and thus to form a conjugation system between the two aromatic rings through the nitrogen atom.

The attenuated total reflectance Fourier transform infrared spectrum of complex **I** grafted on the surface of a TiO₂ film is shown in Figure 2. For clarity of the dye absorption spectrum a TiO₂ reference film heated to 500 °C has been subtracted. The long C₁₄ alkyl chain is readily observed from the CH₂ modes at 2859 & 2925 cm⁻¹, while the peak located at 2961 cm⁻¹ resulted from the stretching mode of the lone CH₃ group. Compared with the corresponding peaks of the powder, the increased sharpness of these peaks on the TiO₂ surface is suggestive of increased ordering of the alkyl chain. The coordinated thiocyanate ligand shows a strong peak at 2104 cm⁻¹, typical of the C=N mode. The intense peak at 1720 cm⁻¹ for the carboxylic acid mode of complex **I** have nearly disappeared after grafting onto the TiO₂ surface. Meanwhile, the appearance of the carboxylate peaks at 1384 & 1600 cm⁻¹ corresponds to the symmetric and asymmetric modes, respectively. These indicate that carboxylic acids are implicated in the surface attachment of the dye. Additionally, The pyridyl ring modes are evident from some sharp lines in the region of 1540–1600 cm⁻¹.

The electronic absorption spectrum (Figure 3) of complex **I** as well as complex **II** shows the characteristic MLCT absorption bands in the visible region like other heteroleptic polypyridyl ruthenium(II) complexes. In acetonitrile and *tert*-butyl alcohol mixture (volume ratio: 1/1), these MLCT transition absorption arise at 568 and 426 nm. The MLCT absorption at 568 nm is 8,700 M⁻¹ cm⁻¹. The intense absorption band at 317 nm in the UV region is due to intra-ligand ($\pi \rightarrow \pi^*$) charge transitions of the dcbpy ligand. When compared with the analogous complexes containing alkyl substituted 2,2'-bipyridine ligands instead of DPA-R, the low energy MLCT band of complex **I** or **II** is lower in the molar extinction coefficient but red shifted by about 25 nm. Thus, it is interesting to extend the conjugated system of DPA-R ligand to enhance the molar extinction coefficient as well as realize panchromatic light-harvesting. The emission spectrum (Figure 3) of complex **I** in the same solvent mixture gives a single broad band centered at 850 nm when excited at 530 nm.

(8) Wang, P.; Zakeeruddin, S. M.; Comte, P.; Charvet, R.; Humphry-Baker, R.; Grätzel, M. *J. Phys. Chem. B* **2003**, *107*, 14336.

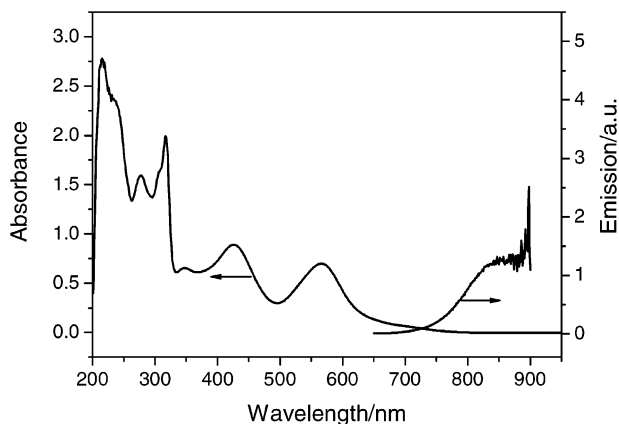


Figure 3. Electronic absorption and emission spectra of complex **I** in the mixture of acetonitrile and *tert*-butyl alcohol (volume ratio: 1/1).

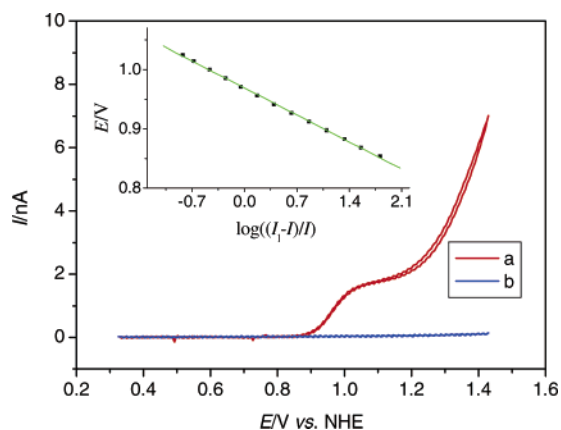


Figure 4. Steady-state voltammograms of a Pt ultramicroelectrode in DMF (a) with and (b) without 2 mM complex **I**. Supporting electrolyte: 0.1 M TBAPF₆; scan rate: 50 mV s⁻¹. The inset shows the relationship between $\log((I_l - I)/I)$ and E .

As shown in Figure 4, a steady-state sigmoid-type curve in the potential range from 0.8 to 1.1 V was obtained with a Pt ultramicroelectrode for the DMF solution containing 2 mM complex **I**, which can be ascribed to the redox process of the ruthenium center. The more positive redox waves resulted from the oxidation of thiocyanate ligand. Thus, the diffusion coefficient (D) of complex **I** molecule was calculated to be $4.6 \times 10^{-6} \text{ cm}^2 \text{ s}^{-1}$ from the limiting current (I_l) due to the redox of ruthenium center by the following equation.⁹

$$I_l = 4nFDca$$

Where n is the electron-transfer number per molecule, F is the Faraday constant, a is the ultramicroelectrode radius, and c is the bulk concentration of electroactive species. The plot of $\log((I_l - I)/I)$ (I_l = limiting current, I = current) vs. potential (E) or so-called log-plot (the inset of Figure 4) is linear with a slope of 62 mV, which is close to the theoretical value of $2.303RT/F$ (59 mV at 25 °C) as expected for a reversible one-electron diffusion-controlled charge-transfer process.⁹ To our knowledge, this is the first polypyridyl ruthenium sensitizer with the thiocyanate ligand having electrochemically reversible behavior, which is normally believed to be a desir-

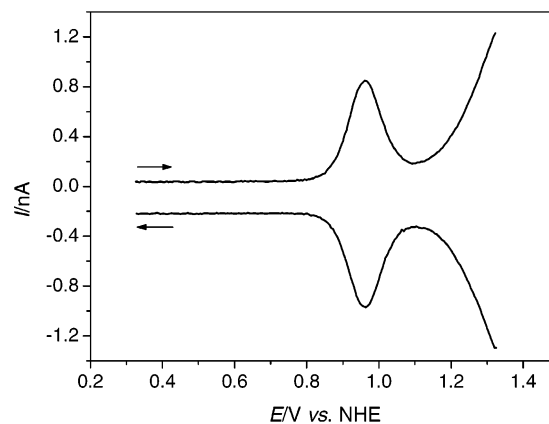


Figure 5. Square-wave voltammograms of a Pt ultramicroelectrode in DMF with 2 mM complex **I**. Supporting electrolyte: 0.1 M TBAPF₆. Potential step increment: 10 mV; frequency: 25 Hz.

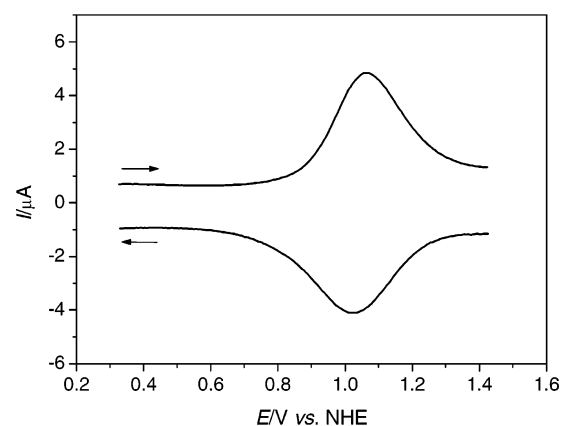


Figure 6. Square-wave voltammograms of a TiO₂ nanocrystalline electrode anchored with complex **I** in DMF. Supporting electrolyte: 0.1 M TBAPF₆. Potential step increment: 10 mV; frequency: 25 Hz.

able property for the device lifetime of DSCs. A further more accurate determination of redox potential was performed by square-wave voltammetry.¹⁰ As presented in Figure 5, the anodic and cathodic peak separation is less than 2 mV while anodic and cathodic peak currents are almost the same, further showing a reversible electrochemical behavior. With Pt as working electrode, the formal potential of complex **I** in DMF was determined to be 0.97 V vs NHE. Figure 6 shows square-wave voltammograms of complex **I** anchored on the surface of TiO₂ nanocrystals. The 40 mV peak-peak separation could be caused by the uncompensated solution ohmic drop or slow tunneling charge-transfer process between conducting glass and complex **I** anchored on TiO₂. The formal redox potential of anchored complex **I** was calculated to be 1.04 V vs NHE by averaging the anodic and cathodic peak potentials. The 70 mV positive shift after anchoring complex **I** onto TiO₂ may be indicative of an electron density decrease on ruthenium center due to a strong electronic coupling between dye molecules and TiO₂ through the carboxylate bridge. This trend was also observed for other heteroleptic polypyridyl ruthenium dyes while their deprotonated forms have lower redox potentials in solution (Wang, P. et al., unpublished

(9) Bard, A. J.; Faulkner, L. R., *Electrochemical Methods: Fundamentals and Applications*, 2nd ed.; Wiley: Weinheim, 2001.

(10) Osteryoung, J.; O'Dea, J. J. In *Electroanalytical Chemistry*; Bard, A. J., Ed.; Marcel Dekker: New York, 1986; Vol. 14, pp 209–308.

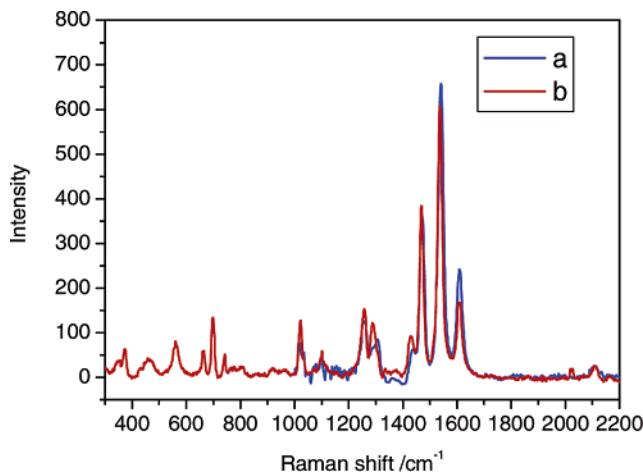


Figure 7. Resonance Raman spectra of (a) complex **I** covered TiO_2 film and (b) sealed DSC.

results.). To some extent, this may be related to the ultrafast electron injection from the light-harvesting center to the TiO_2 semiconductor.

To design new efficient sensitizers for DSCs, it is very important to know in heteroleptic ruthenium complexes where the LUMO is localized. Resonant Raman spectroscopy is a powerful probe for obtaining ground and excited state properties of dye chromophores. Although the ground state is probed, the vibrational modes are resonantly enhanced due to coupling with the electronic MLCT transition. After mapping the resonant Raman spectrum with the electronic absorption spectrum by varying the incident frequency, the ligand associated with the LUMO can be identified. The Raman excitation of the MLCT band indicates a major displacement of charge to the ligand.¹¹ In complexes **I** and **II** laser-excitation at 482.5 nm showed bands characteristic of both types of ligands (DPA-R) and dcbpy. However when excited at 520.8 nm only the vibrational modes corresponding to the dcbpy ligand were observed at 1607, 1535, 1467, 1257, and 1021 cm^{-1} as shown in curve b of Figure 7. Thus, the LUMO of complexes **I** and **II** is located on the dcbpy ligand that also serves as an anchoring ligand in DSCs. The conclusion obtained based on the resonance Raman experiments is consistent with the previously reported electrochemical study of DPA-R and dcbpy complexes.^{5b} Additionally, the weak bands at 2107 cm^{-1} and 798 cm^{-1} are due to the $\nu(\text{N}=\text{C})$ and $\nu(\text{C}=\text{S})$ stretching vibrations, respectively. The metal-nitrogen vibrational modes $\nu(\text{M}-\text{N})$ were observed in the 360 cm^{-1} region. The Raman spectrum of complex **I** on anatase shows a nearly identical spectrum to the dye in a sealed working cell. The diagnostic peak positions have not varied. Only the peak at 1291 cm^{-1} is different, probably due to the intensity change of the symmetric carboxylic mode due to a pH change of the TiO_2 surface in the presence of electrolyte. A small difference in peak intensity probably reflects a change in the medium dielectric.

Upon irradiation, sensitizers adsorbed on the surface of a wide band gap metal oxide semiconductor may readily inject electrons into the conduction band of the solid. Charge injection has been found for numerous efficient systems to be a very fast process that occurs

(11) Fuchs, Y.; Lofters, S.; Dieter, T.; Shi, W.; Morgan, R.; Streckas, T. C.; Gafney, H.; Baker, A. D. *J. Am. Chem. Soc.* **1987**, *109*, 2691.

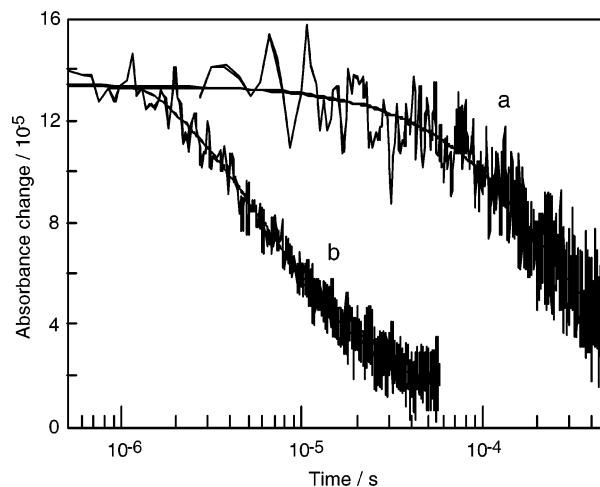


Figure 8. Transient absorbance decay kinetics of the oxidized state of complex **I** adsorbed on a nanocrystalline TiO_2 film in the presence of (a) pure solvent of acetonitrile/valeronitrile (volume ratio: 3:1) and (b) iodide/tri-iodide based electrolyte used for photovoltaic device. Absorbance changes were measured at a probe wavelength of 650 nm, employing 543-nm laser excitation (5 ns fwhm pulse duration, $10 \mu\text{J cm}^{-2}$ pulse fluence).

in the femtosecond time frame.¹² In the absence of electrolytes, the injected electrons trapped in the conduction band recombine with the oxidized-state dye molecules (S^+) slowly, typically in the microsecond-millisecond domain.¹³ In photoelectrochemical energy conversion devices employing dye-sensitized TiO_2 mesoporous electrodes, this charge transfer process may be intercepted by iodide in the electrolytes. The efficiency of charge separation in DSCs is directly controlled by the kinetic competition between the charge recombination and dye regeneration reactions taking place between oxidized state dye molecules and electrons trapped in the semiconductor conduction band, and between oxidized state dye molecules and iodide in the electrolyte, respectively. Here nanosecond time-resolved laser experiments¹⁴ were employed to scrutinize the dynamics of these two charge-transfer processes when complex **I** was used as sensitizer. Transient absorbance measured above 620 nm, following photo-induced electron injection into the semiconductor film, is due to the ligand-to-metal charge transfer (LMCT) transitions, which is characteristic of the oxidized polypyridyl ruthenium(III) complex with the thiocyanate ligand.¹⁵ In the absence of a redox mediator (Figure 8, trace a), the decay of the absorption signal recorded at 650 nm reflects the dynamics of recombina-

(12) (a) Rehm, J. M.; Mclondon, G. L.; Nagasawa, Y.; Yoshihara, K.; Moser, J. E.; Grätzel, M. *J. Phys. Chem.* **1996**, *100*, 2820. (b) Burfeindt, B.; Hannappel, T.; Storck, W.; Willig, F. *J. Phys. Chem.* **1996**, *100*, 16463. (c) Asbury, J. B.; Ellingson, R. J.; Ghosh, H. N.; Ferrere, S.; Nozik, A. J.; Lian, T. *J. Phys. Chem. B* **1999**, *103*, 3110. (d) Hilgendorff, M.; Sundström, V. *J. Phys. Chem. B* **1998**, *102*, 10505. (e) Moser, J. E.; Wolf, M.; Lenzmann, F.; Grätzel, M. *Z. Phys. Chem.* **1999**, *212*, 85.

(13) (a) O'Regan, B.; Moser, J. E.; Anderson, M.; Grätzel, M. *J. Phys. Chem.* **1990**, *94*, 8720. (b) Haque, S. A.; Tachibana, Y.; Klug, D. R.; Durrant, J. R. *J. Phys. Chem. B* **1998**, *102*, 1745.

(14) (a) Pelet, S.; Moser, J. E.; Grätzel, M. *J. Phys. Chem. B* **2000**, *104*, 1791. (b) Wang, P.; Zakeeruddin, S. M.; Moser, J. E.; Grätzel, M. *J. Phys. Chem. B* **2003**, *107*, 13280.

(15) (a) Tachibana, Y.; Moser, J. E.; Grätzel, M.; Klug, D. R.; Durrant, J. R. *J. Phys. Chem.* **1996**, *100*, 20056. (b) Moser, J. E.; Noukakis, D.; Bach, U.; Tachibana, Y.; Klug, D. R.; Durrant, J. R.; Humphry-Baker, R.; Grätzel, M. *J. Phys. Chem. B* **1998**, *102*, 3649.

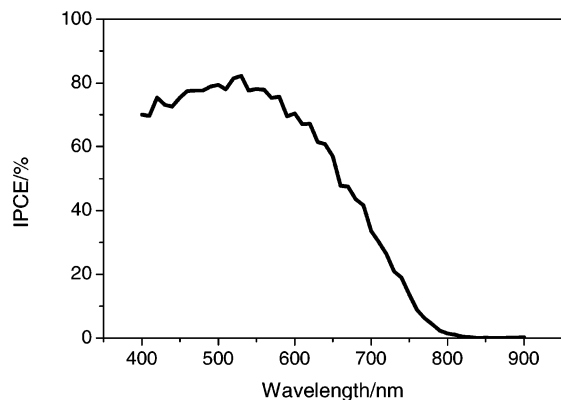


Figure 9. Typical photocurrent action spectrum of photovoltaic devices based on 18 μm thick nanocrystalline TiO_2 film sensitized with complex **I**. Cell active area: 0.158 cm^2 .

tion of injected electrons with the oxidized dye (S^+), having a $t_{1/2}$ of 200 μs . The charge recombination kinetics for complex **I** are comparable to what has been reported for the standard N-719 dye ($t_{1/2} = 250 \mu\text{s}$).^{14a} In the presence of the iodide electrolyte, the decay of the oxidized dye signal was significantly accelerated with $t_{1/2} = 8 \mu\text{s}$, showing that back electron transfer was indeed intercepted by the mediator (Figure 8, trace b). However, the same process takes place more than 1 order of magnitude faster ($t_{1/2} = 600 \text{ ns}$) for the N-719 dye.^{14a} Slower dye regeneration of Complex **I** compared with the N-719 dye implies that more conduction band electrons can undergo recombination with some of the initial S^+ species and thus escape from photocurrent collection. The long aliphatic chain carried by Complex **I** is expected to increase the minimum approach distance between iodide and the ruthenium center or the thiocyanate ligand and hence decrease the dye regeneration rate. This phenomenon has also been observed for other types of heteroleptic polypyridyl ruthenium sensitizers.^{6a}

Figure 9 shows the typical photocurrent action spectra of DSCs with complex **I**, where the incident photon to current conversion efficiency (IPCE) is plotted as a function of wavelength. The broad feature appears covering almost the entire visible spectrum, with a maximum peak value of about 80% at a 530-nm wavelength. Excluding the light absorption and diffraction loss by the conducting glass, the maximum efficiency of absorbent photon to current conversion efficiency is over 90%. Figure 10 presents current density–voltage characteristics of a DSC with complex **I** at AM 1.5 illuminations and under dark. The detailed device parameters are listed in Table 1. The short-circuit photocurrent density (J_{sc}), open-circuit photovoltage (V_{oc}), and fill factor (ff) of devices with complex **I** under AM 1.5 full sunlight are 15.5 mA cm^{-2} , 756 mV, and 0.70, respectively, yielding an overall conversion efficiency (η) of 8.2%, which is comparable with other types of amphiphilic ruthenium sensitizers.¹⁶ At lower incident light intensities, overall power conversion efficiencies are close to 9%. Note that this unoptimized device has been tested with a mask that completely stops the diffusive light. With the same TiO_2 electrode

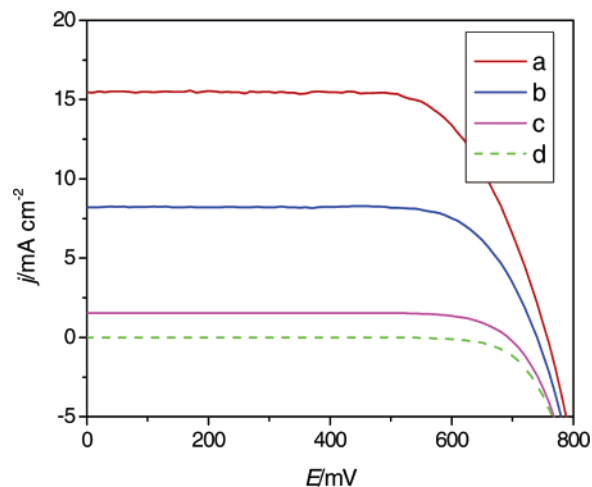


Figure 10. Current density–voltage characteristics of photovoltaic devices with complex **I** as a sensitizer at AM 1.5 illuminations (light intensities for curves a to c: 99.7, 52.1 and 9.5 mW cm^{-2} , respectively) and under dark (curve d). Cell active area: 0.158 cm^2 .

Table 1. Detailed Photovoltaic Parameters of DSCs with Complex **I under Different Incident Light Intensities^a**

$P_{\text{in}}/\text{mW cm}^{-2}$	$J_{\text{sc}}/\text{mA cm}^{-2}$	V_{oc}/mV	$P_{\text{max}}/\text{mW cm}^{-2}$	ff	$\eta/\%$
9.5	1.54	692	0.84	0.786	8.8
52.1	8.38	740	4.53	0.745	8.7
99.7	15.5	756	8.21	0.702	8.2

^a The spectral distribution of the lamp simulates air mass 1.5 solar light. Incident power intensity: P_{in} ; short-circuit photocurrent density: J_{sc} ; open-circuit photovoltage: V_{oc} ; maximum electricity output power density: P_{max} ; fill factor: $ff = P_{\text{max}}/P_{\text{in}}$; total power conversion efficiency: η ; cell active area: 0.158 cm^2 .

and electrolyte, the standard N-719 dye is relatively about 14% more efficient at AM 1.5 full sunlight. As the molar extinction coefficient of complex **I** is lower compared with that of the N-719 dye, it is possible to get higher efficiencies with a thicker TiO_2 film.

Conclusions

In summary, two new amphiphilic polypyridyl ruthenium complexes $[\text{Ru}(\text{dcbpy})(\text{L})(\text{NCS})_2]$, where dcbpy is 4,4'-dicarboxylic acid-2,2'-bipyridine and L is *N,N*-di(2-pyridyl)-dodecylamine or *N,N*-di(2-pyridyl)-tetradecylamine) were synthesized and systematically characterized by electrochemical and spectroscopic methods. Electrochemical studies have revealed that the oxidized state of this new type of dye is more stable than other polypyridyl ruthenium sensitizers with the thiocyanate ligand. Furthermore, these amphiphilic ruthenium complexes have been successfully used as sensitizers for nanocrystalline dye-sensitized solar cells with efficiencies of 8.2% at an 100 mW cm^{-2} irradiance of air mass 1.5 solar light and $\geq 8.7\%$ at lower light intensities. The further work will be targeted to extend the conjugated system of the DPA-R ligand and thus to enhance the light-harvesting efficiency.

Acknowledgment. We are grateful to T. Koyanagi (CCIC, Japan) for providing the 400 nm TiO_2 particles and P. Comte for the mesoporous film preparation. The Swiss Science Foundation, Swiss Federal Office for Energy (OFEN), and the European Office of U.S. Air Force under Contract No. F61775-00-C0003 have supported this work.

CM0498710

(16) Zakeeruddin, S. M.; Nazeeruddin, M. K.; Humphry-Baker, R.; Péchy, P.; Quagliotto, P.; Barolo, C.; Viscard, G.; Grätzel, M. *Langmuir* **2002**, *18*, 952.